Multiscale analysis of geometric planar deformations: application to wild animals electronic tracking and satellite ocean observation data

Ronan Fablet, Alexis Chaigneau, Sophie Bertrand

Multiscale analysis of geometric planar deformations: application to wild animals electronic tracking and satellite ocean observation data

Ronan Fablet, *Senior Member, IEEE,* Alexis Chaigneau and Sophie Bertrand,

Abstract

The development of animal tracking technologies (including for instance GPS and ARGOS satellite systems) and the increasing resolution of remote sensing observations call for tools extracting and describing the geometric patterns along a track or within an image over a wide range of spatial scales. Whereas shape analysis has largely been addressed over the last decades, the multiscale analysis of the geometry of opened planar curves has received little attention. We here show that classical multiscale techniques cannot properly address this issue and propose an original wavelet-based scheme. To highlight the generic nature of our multiscale wavelet technique, we report applications to two different observation datasets, namely wild animal movement paths recorded by electronic tags and satellite observations of sea surface geophysical fields.

I. Introduction

The analysis of trajectory data is a particularly active research domain. While the reconstruction of trajectories initially retained most of the attention, trajectory characterization and modeling are now among the key issues in numerous areas. For instance, in the field of ecological sciences, the development of miniaturized high-resolution GPS tracking devices [19], [23], [27], [46], [61] initiated the investigation of poorly known behaviors of wild animals (e.g., foraging activity or migratory displacements), such as sea turtles, sharks, seabirds, marine and terrestrial mammals, etc. We show in Fig.1 an example of a GPS track from a Peruvian booby (*Sula variegata*) foraging off its breeding colony. It involves oscillations and loop patterns with spatial scales varying from tens of meters to a few kilometers. The 1-to-100m looping patterns are generally interpreted as area restricted searches (ARS) for prey [19] whereas larger scales patterns might be driven by flight constraints or by the tracking of specific physical

R. Fablet is with the Department of Signal and Communications, Institut Telecom/Telecom Bretagne; UMR LabSTICC ; Technopôle Brest-Iroise, Brest, France, email: ronan.fablet@telecom-bretagne.eu.

A. Chaigneau is with IRD/UMR LEGOS, Av. E. Belin, Toulouse, France, email: alexis.chaigneau@ird.fr

S. Bertrand is with IRD/UMR EME, Av. Jean Monnet, Sète, France, email: sophie.bertrand@ird.fr

structures at the ocean surface [56]. This example provides a typical illustration of the wide range of nested scales observed along wild animal movement paths. Numerous other research areas involve similar multiscale geometric patterns along movement paths and planar curves. One may cite other satellite-based tracking applications, such as satellite-tracked drifters at the ocean surface, fishing vessel and maritime traffic surveillance [7], video-surveillance and video indexing applications [25], [50] as well as the characterization of the geometry of geophysical fields [5], [1], [24].

These different examples stress the need for tools dedicated to the multiscale analysis of the geometric deformations along planar curves. Though the analysis of two-dimensional (2D) shapes and trajectories has been an active research topic, especially for matching and classification applications [9], [15], [50], [64], we address here important methodological contributions which were not dealt with in previous works:

- a wavelet-based scale-space decomposition of the geometry of opened planar curves;
- the extraction of significant multiscale geometric patterns along opened planar curves.

To highlight the relevance of the proposed wavelet-based technique, we apply this methodology (1) to the analysis of GPS tracks of seabird movements and (2) to the characterization of the geometry of remotely sensed sea surface geophysical fields. This paper is organized as follows. Problem statement and previous works are discussed in Section II. Section III presents the proposed wavelet-based analysis of the geometry of opened planar curves. The applications to seabird GPS tracks and ocean-surface geophysical fields are reported in Sections V and VI. Key aspects of our contributions and future work are further discussed in Section VII.

II. Problem statement and related work

The analysis of 2D trajectories is a particularly active research theme in ecology. In their proposition for a 'movement ecology paradigm', Nathan et al. (2008) identified four major data analysis challenges: (1) parsing the movement path into a string of elemental units, (2) classifying path segments as basic functional units of the track, (3) quantifying the environmental signal affecting moving organisms, (4) assessing how processes operating at multiple spatiotemporal scales determine the composition of movements phases and their frequency in its track. Regarding the first challenge, methods addressed the identification of areas of special interest within the trajectory, especially probable feeding spots corresponding to areas of restricted searches (ARS, [19]). ARS have been classically identified from the analysis of local sinuosity indexes along the track. The First-Passage-Time (FPT, Fig. 1)) index is probably the most popular [19]. At any position p of the track, this index is computed as the duration of the track segment around p comprised in a circular region centered in p. The radius of the circular region, which is typically selected as a local maximum of the variance of the FPT calculation, defines a single scale of analysis and depends on the analyst's expertise. The same remark holds for other sinuosity indexes, such as fractal landscape, residence time and moving average (see [32] for a brief review). The second challenge has been mostly addressed through state-space models (e.g. [31]). These models aim at partitioning the trajectory into a sequence of behavioural states from local state-specific properties of the movement path (i.e. turning angles, speeds, etc.). Due to their sequential nature, such local properties cannot however address multiscale nested patterns. The third and fourth challenges have received

little attention and may be actually quite interdependent. Natural ecosystems are made of heterogeneous spaces with nested structures of multiple characteristic scales in hierarchical interaction. For instance, small pelagic forage fish, upon which seabird like boobies commonly feed, are organized in nested collective structures [22]: schools, clusters of schools, clusters of clusters. Seabirds foraging on such constantly moving pelagic fish need to track down their distribution and their movements should then reflect to some extent the hierarchical organization of forage fish (e.g. [19]). Multi-fractal approaches [23] provide a global characterization of the geometry of a trajectory for different scale ranges. However, they cannot localize the multi-scale patterns of interest along a track. The core of our contribution is precisely to shift from single-scale approaches to a multiscale analysis of the geometry of trajectory data.

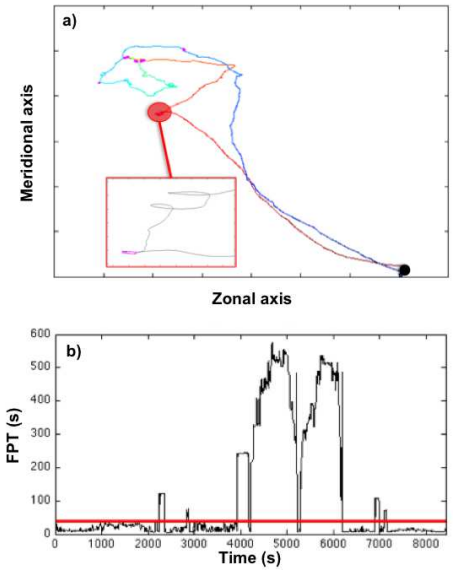

Fig. 1. **FPT (First-Time Passage) analysis of a trajectory**: GPS track of the foraging trip of a Peruvian booby sampled every second and detected movement patterns using the FPT approach [19] for an analyzing scale set to 40m with a zoom on a segment involving undetected patterns, the color along the track refers to the cumulated time from the beginning of the track (top); series of the FPT index (see text for details) along the track for a 40m analyzing scale with the threshold set empirically for movement pattern detection (bottom). The FPT analysis being a single-scale scheme, it cannot identify all loop-like and oscillation-like patterns of interest.

From a computer vision perspective, the analysis of 2D shapes has long been an active research theme and quite a few studies addressed the multiscale decomposition of planar shapes, e.g. [15], [64]. Among others, one may cite shape decomposition techniques, such as Fourier and Zernike moments [64]. Such techniques assume stationarity and closed planar curves. Curvature space-scale [15] was also developed to provide a multiscale representation of a planar curve. It relies on the iterative smoothing and interpolation of the curve at different scales. Mainly considered for shape recognition and classification, the curvature space-scale was generally used to represent a curve as the zero-crossings of the curvature along the curve, *i.e* points at which the curvature is zero, at different scales. Though this scheme applies to opened planar curves, it does not actually address the two main issues

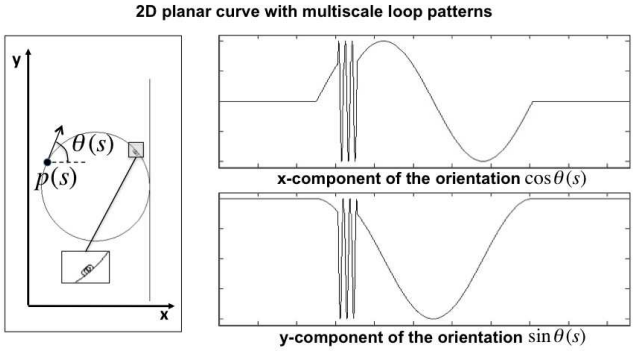

Fig. 2. **Multi-scale analysis of the geometry of a planar curve as a time-frequency decomposition of its orientation series**: planar curve involving loop structures at two different scales (upper panel), the series of the x- and y- component of the direction of the tangent to the curve, i.e. series $cos\theta(s)$ and $sin\theta(s)$ of the orientation $\theta(s)$ of the tangent to the curve as a function of the curvilinear abscissa s, depicts frequency modulations associated with the scale of the loop structures (lower panel).

considered here, the determination of the characteristic scales of a planar curve and the detection of patterns of interest along a curve. Recently, shape matching criteria [9], [26] were proven robust for classification and clustering issues, and applications to trajectory analysis have been considered [50]. They typically resort to the computation of mean trajectories, for instance to detect abnormal behaviors. These criteria however hardly apply to the multi-scale characterization of local patterns along a trajectory as targeted here.

This brief review points out that the state-of-the-art approaches in the field of trajectory and 2D shape analysis cannot address satisfactorily the multiscale characterization and extraction of geometric patterns of interest along any arbitrary planar curve. In this work, we address these issues and develop a novel multiscale wavelet-based decomposition of the geometry of planar curves

III. Multiscale wavelet-based decomposition of the geometry of planar curves

This section details the proposed framework for the multiscale decomposition of the geometry planar curves. Let us denote by s the curvilinear abscissa along a planar curve $\mathcal{C}$ and $\{(x(s), y(s)\}$ the parameterization of the x and y coordinates of the position along the curve w.r.t. (with respect to) the curvilinear abscissa in the considered Cartesian planar coordinate system. Numerically, we consider a discrete version $\{(x(s_k), y(s_k)\}_k$ of the curve $\mathcal{C}$ with equally sampled points w.r.t. curvilinear abscissa s.

A. Principle

Our approach is based on the following observation. For a planar curve consisting of a series of loops at different scales, the series of the x and y components of the local tangent to the curve w.r.t. the curvilinear abscissa are quadrature sinusoidal components (Fig.2). The characteristic period P of the sinusoidal modulation of the orientation series relates to the radius R of the loop as $R = P/2\pi$. Oscillation-like patterns involve similar frequency modulations with the same relation between the mean curvature radius of the oscillation and its characteristic period.

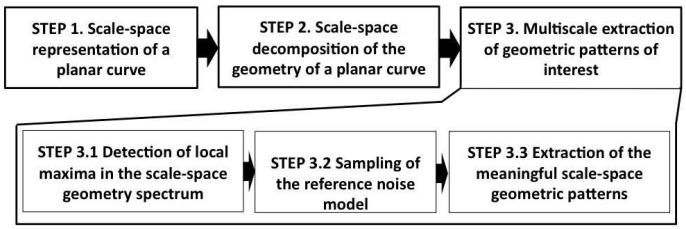

Fig. 3. **Functional sketch of the proposed framework for the multiscale analysis and extraction of the geometric patterns of a planar curve**: it involves three main steps (1) a scale-space representation of the planar curve (Section III-B), (2) a scale-space decomposition of the geometry of a planar curve (Section III-C) and (3) a multiscale extraction of geometric patterns of interest IV-B. This third step comprises three sub-steps: (3.1) the detection of local maxima in the processed scale-space geometry spectrum, (3.2) the sampling of a reference noise model, (3.3) the extraction of the meaningful scale-space geometric patterns.

These observations provide the basis for the characterization of the local geometry of a planar curve from the time-frequency analysis of the series of the orientation of the tangent to the curve. The multiscale nature of the geometric patterns requires considering with care this time-frequency analysis as detailed in the next section. The general functional sketch of the proposed framework involves three main aspects (Fig.3). We first compute a scale-space representation of the processed planar curve (Section III-B). In a second step, we extract a scale-space decomposition of the geometry of a planar curve (Section III-C). Given this scale-space decomposition, we achieve a multiscale extraction of geometric patterns of interest (Section IV). This third step comprises three sub-steps: the detection of local maxima in the processed scale-space geometry spectrum, the sampling of a reference noise model and the extraction of the meaningful scale-space geometric patterns.

B. Scale-space representation of a planar curve

Among commonly used time-frequency decompositions of a 1D signal, two main categories can be distinguished. The first category, including for instance Wigner-Wille and wavelet transforms [20], typically relies on the projection of the signal onto time-frequency dictionaries, each atom or function of the dictionary referring to a predefined time-frequency domain, *i.e.* predefined time intervals and frequency bands. The second category exploits non-parametric decompositions, the most popular being the empirical mode decomposition (EMD) [21]. The EMD relies on the decomposition of the signal onto a set of intrinsic mode functions, each intrinsic mode function being estimated from the signal itself and corresponding to a simple oscillatory mode, *i.e.* the counterpart of the harmonic functions used in the first category of time-frequency techniques. None of these two categories of time-frequency decompositions however straightforwardly apply to 2D planar curves for which no ”time” reference common to all scales exist as explained below. Here the classical time index is replaced by the curvilinear abscissa. However whereas small-scale patterns in a 1D signal x only affect the values taken by x, in the case of a curve they affect both the curvilinear abscissa and the series of the orientation of the tangent to the curve. For two curves sharing the same large-scale patterns between two points, the one with greater small-scale variabilities involves a larger cumulated distance between these two points. The small-scale noise-like patterns then result in noisy orientation series as well as in

distortions of the curvilinear abscissa which plays the role of a time index in our analysis. Whereas time-frequency analysis tools can address the first effect, they assume that no scale-dependent distortion of this "curvilinear time" axis occurs. These issues are further illustrated and discussed through numerical simulations (Section III-D, Fig.4).

To overcome these two effects requires us to consider a scale-space representation of the curve [15] prior (or jointly) to the scale-space decomposition of its geometry. We adapt the standard scale-space representation of a 2D shape [15] to opened planar curves. As they may involve loop patterns and self-intersections, the application of the classical scale-space representation of a curve [15] results in local singularities. To address this issue, we combine a kernel-based smoothing to a morphological analysis as follows. We first detect the elementary loops of the curve from the set of all the self-intersections of the curve. Elementary loops are formally defined as curve segments whose origin does not belong to a smaller elementary loop. At any scale a, the scale-space representation of the curve consists first in applying a morphological filter which removes all the elementary loops of radius smaller than $a/2\pi$ and second in performing a Gaussian smoothing with a variance set to a^2 similarly to the classical shape scale-space [15].

We denote by $\{\mathcal{C}_a\}$ the scale-space representation of curve $\mathcal{C}$, $\mathcal{C}_a$ being the representation of the curve at scale a.

C. Scale-space decomposition of the geometry of planar curves

As stressed in the previous section, we are required to jointly consider a scale-space representation of the curve and the time-frequency analysis of its orientation series. This motivates our choice for a parametric time-frequency method, namely a continuous wavelet transform (CWT) [57]. Formally, the CWT of a 1D signal z consists in computing complex wavelet coefficients $\{w_z(a,\tau)\}$ as the convolution of the signal by scaled and translated versions of the mother wavelet Ψ

$$w_z(a,\tau) = \frac{1}{\sqrt{a}} \int_{-\infty}^{+\infty} z(t) \cdot \Psi^* \left(\frac{t-\tau}{a} \right) dt \tag{1}$$

where a is the scale, t and τ time indices and u^* stands for the conjugate complex of complex value u. The mother wavelet considered here is the complex Morlet wavelet, which is particularly suited to the analysis of frequency modulations [41], [57], and realizes a good time-frequency trade-off, *i.e.* the trade-off between correct estimations in the time domain and in the frequency domain [41]. The Morlet wavelet is defined from a plane wave weighted by a Gaussian window

$$\Psi_{\sigma_0}(s) = \left(e^{2i\pi s} - e^{-\frac{\sigma_0^2}{2}} \right) e^{-2\pi \frac{s^2}{\sigma_0^2}} \tag{2}$$

The parameter σ_0 balances time and frequency resolutions. Conventionally, σ_0 should be strictly greater than 5 to avoid numerical issues at high time resolution [41], [57]. In the reported experiments, we use the classical parameterization $\sigma_0 = 6$ [57]. σ_0 values taken in the range $]5, 8]$ led to similar experimental results (not shown here).

As a direct application, we first compute the CWT of the series of the orientations θ along the curve through a complex representation z of these orientations, *i.e.* $z(s) = \cos\theta(s) + i\dot{\sin}\theta(s)$ for any position s along the curve.

However, as mentioned above, this direct application of the CWT to orientation series z does not address the distortions of the large-scale patterns caused by finer-scale ones (see Fig.4).

To address these issues, the complex wavelet coefficients are computed for the orientation series of a scale-space representation of the curve. More precisely, the computation of wavelet coefficients at scale a are computed for an orientation series corresponding to a smoothed version of the curve for which fine-scale structures (w.r.t. analysis radius $R = a/2\pi$) have been smoothed out. Formally, we resort to the definition of the complex wavelet coefficients $w_{\mathcal{C}}(a_R, \tau_R)$ of curve C at scale a_R and position τ_R as

$$w_{\mathcal{C}}(a_R, \tau_R) = \frac{1}{\sqrt{a_R}} \int_{-\infty}^{+\infty} z_{\mathcal{C}_{b_R}}(t_R) \cdot \Psi^* \left(\frac{t_R - \tau_R}{a_R} \right) dt_R \tag{3}$$

where scale a_R is parameterized as $a_R = 2\pi R$ w.r.t. analysis radius R, $z_{\mathcal{C}_{b_R}}$ the complex representation of the series of the orientations of curve $\mathcal{C}_{b_R}$, the curve of the scale-space representation of curve $\mathcal{C}$ at scale b_R. We typically set $b_R = a_R/10$ to balance between the scale resolution of the wavelet analysis and the filtering of fine-scale structures (at scale a_R). τ_R and t_R denote positions, parameterized by the curvilinear abscissa along curve $\mathcal{C}_{\mathcal{R}}$.

Given wavelet coefficients $w_{\mathcal{C}}(a_R, \tau_R)$, the power spectrum of the scale-space decomposition is defined as $|w_{\mathcal{C}}(a_R, \tau_R)|^2$. Index τ_R being computed as the curvilinear abscissa along curve $\mathcal{C}_{\mathcal{R}}$, linear interpolations are applied to compute a power spectrum $S_{\mathcal{C}}(a_R, \tau)$ referenced w.r.t. the curvilinear abscissa of the original curve $\mathcal{C}$. Let us denote by $S_{\mathcal{C}}$ this wavelet power spectrum referred to as the scale-space spectrum of the geometry of planar curve $\mathcal{C}$. The presence of a looping or oscillating pattern of mean radius R at position τ results in large energy values in $S_{\mathcal{C}}$ in the neighborhood of the scale-space position $(a_R = 2\pi R, \tau_R)$. Additionally, we also evaluate the cone of influence of the spectrum, i.e. the region of the scale-space domain free of edge effects [57].

D. Illustration using simulated curves

We first carry out a quantitative evaluation of the proposed approach from simulated trajectories composed of two successive large loops of radius 81.5km, the first one containing three successive loops of radius 5.1km. In addition, a fine-scale geometric noise is considered according to:

$$\begin{cases} x_B(t) &= \alpha * [sin(2 * \pi * w * t) + u_t] \\ y_B(t) &= \alpha * [v_t] \end{cases} \tag{4}$$

where (x_B,y_B) are the x and y components of the noise, w the frequency of the fine-scale oscillations, u_t and v_t are samples drawn from a centered Gaussian distribution with unit variance. The noise level is given by parameter α. Fig.4 reports the comparison of the multiscale characterization of the geometry of the trajectory derived from i) the direct application of a time-frequency decomposition of the orientation series of the curve (Eq.1) (Fig.4, panel B, left) and ii) the proposed approach (Eq.3) (Fig.4, panel B, right). The considered parameter setting involves $\alpha = 1$ and $b_R = a_R/10$ (Eq.3).

The scale-space spectra reported in (Fig.4, second row) stresses the requirement for considering a scale-space representation of the curve jointly to the time-frequency analysis of its orientation series. If we directly apply the CWT to the orientation series of the original curve (Eq.1) (Fig.4, panel B, left), the resulting scale-space geometry

spectrum comprises three different patterns. Below radius of 5.1km, we reveal the fine-scale geometric patterns associated with the simulated geometric noise (x_B, y_B). This spectrum also involves two high-energy regions corresponding to the small and large loop patterns. These patterns are correctly localized in time, but their detection presents a scale bias as well as lower energy values than expected. Whereas the weakening of the energy values may be due to noisy orientation values, the scale bias is related to the fine-scale noise on the curvilinear abscissa of the curve, the latter being the reference time index for the time-frequency decomposition. In contrast, the combination of a scale-space representation of the curve and the time-frequency analysis of the associated orientation series allows to correctly localize loop patterns with good energy values.

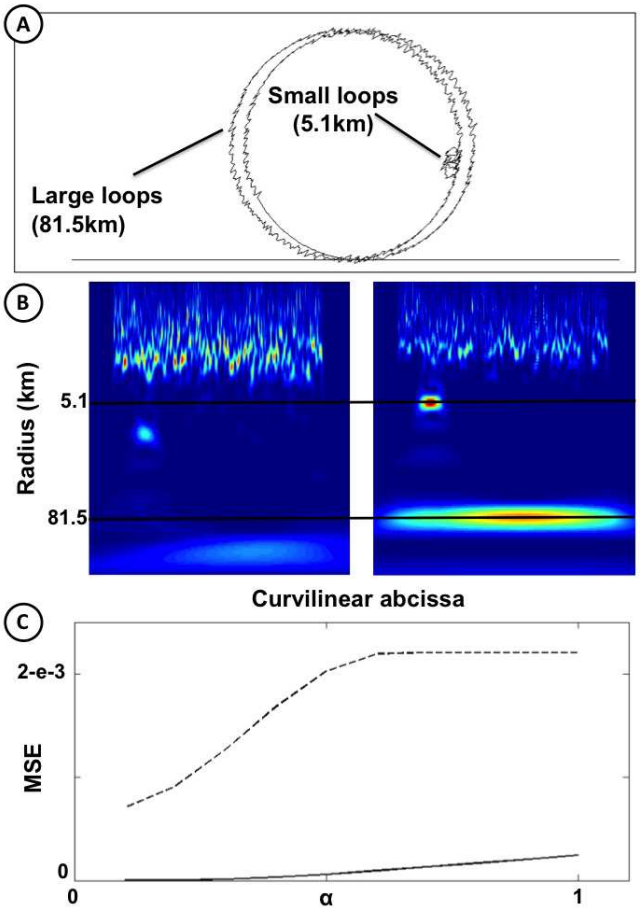

Fig. 4. **Experiments on simulated multiscale trajectories**: for a planar curve depicting two large loops (radius of 81.5km), three small ones (radius of 5.1km) and a fine-scale geometric noise (panel A), the continuous wavelet decomposition(CWT) of the series of the orientations of the tangent to the curve (Eq.1) cannot reveal the presence of the loop patterns due to occlusion effects associated with the presence of the fine-scale noise. By contrast, the proposed approach which combines the CWT to a scale-space representation of the curve (Eq.3) actually allows their identification. We report the scale-space power spectra formed by the magnitude of the computed wavelet coefficients for each method (panel B). We also compare these spectra to the theoretical noise-free power spectrum in terms of mean square error (MSE) for different noise levels, i.e. α (Eq.4) ranging from 0 to 1 (panel C).

A quantitative experiment confirms this qualitative evaluation. Using a mean square error criterion, we compare

the theoretical noise-free geometry spectrum of a curve comprising only the loop patterns with the geometry spectra computed using the two methods (Eq.1) and (Eq.3) for different noise levels. The noise level is parameterized by parameter α (Eq.4) ranging from 0 to 1. Reported results (Fig.4, panel C) point out the relevance of our contribution. As pointed out in the previous section, the filtering scale b_R is set as a trade-off between the filtering of fine-scale patterns (w.r.t. analyzing radius R) and the scale resolution of the wavelet analysis. We considered here $b_R = a_R/10$. Additional experiments not reported here show that the parameterization of the filtering scale b_R in (Eq.3) from $b_R = a_R/10$ to $b_R = a_R/20$ leads to similar results. They motivate the choice of $b_R = a_R/10$ considered in the reported applications to the analysis of wild animal movement paths and remotely sensed sea surface geophysical fields.

IV. Multiscale characterization of geometric patterns along planar curves

We exploit the scale-space decomposition of the geometry of a planar curve (Eq.3) to extract and characterize its key geometric patterns. We introduce the multiscale energy spectrum of the geometric patterns of a planar curve (Section IV-A) and a multiscale extraction of its significant geometric patterns (Section IV-B).

A. Multiscale energy spectrum of the geometric patterns

To describe the characteristic scales of the geometric deformations along a planar curve $\mathcal{C}$, we compute the distribution across scales $D_{\mathcal{C}}$ of the total energy in each scale subband of spectrum $S_{\mathcal{C}}$

$$D_{\mathcal{C}}(R) = \int_{-\infty}^{+\infty} S_{\mathcal{C}}(a_R, \tau_R) d\tau_R \tag{5}$$

For a given radius R, the energy $D_{\mathcal{C}}(R)$ refers to the total energy of the frequency modulations observed along orientation series z with a characteristic period $2\pi R$. It relates to the cumulated distance along the curve in structures with characteristic radius R. Distribution $D_{\mathcal{C}}$ then provides us the mean for identifying characteristic scales, which correspond to local maxima and/or modes of distribution $D_{\mathcal{C}}$.

B. Multiscale extraction of geometric structures of interest

As illustrated in Fig.4, any looping or oscillating pattern along a curve is associated with large energy values in the scale-space geometry spectrum $S_{\mathcal{C}}$ of the planar curve $\mathcal{C}$. We thus aim at detecting such patterns of interest by extracting regions of spectrum $S_{\mathcal{C}}$ depicting significant energy values. The proposed scheme involves three substeps (Fig.3):

- *Step 3.1: the detection of local energy maxima in scale-space spectrum $S_{\mathcal{C}}$*. A scale-space location is a maximum if none of the neighboring locations depict greater energy values. We typically consider 7x7 neighborhoods to prevent from over-detections in flat spectrum regions.
- *Step 3.2: the determination of the scale-space spectrum of the noise reference*. We test the meaningfulness of local regions of the scale-space geometry spectrum $S_{\mathcal{C}}$ in terms of energy levels w.r.t. the energy levels that would be generated by an unstructured random curve with the same turning angle statistics. Formally, this *a*

priori noise model is stated as a first-order correlated random walk [59]. It can be regarded as an adaption to planar curves of the first-order autoregressive model generally considered as the null hypothesis in statistical time series analysis [57]. This noise model is parameterized from the turning angle statistics of curve $\mathcal{C}$.The sampling of the noise model resorts to sampling a turning angle series from the empirical turning angle statistics observed for curve $\mathcal{C}$. A discrete integration of the sampled turning angle series provides the simulated planar curve. From random simulations (typically 200) of this noise model, we estimate the 90^{th} percentile, denoted by $S_{90^{th}}$, of the scale-space geometry spectrum of the noise model. Spectrum $S_{90^{th}}$, provides a noise reference to test whether observed energy values in scale-space spectrum $S_{\mathcal{C}}$ are significant or regarded as noise patterns.

- *Step 3.3: the detection of the significant scale-space geometric patterns.* Given the local energy maxima extracted in Step A, we select those with significant energy values compared to the noise reference $S_{90^{th}}$ at the same scale-space locations. For any local maximum, we determine the associated region of spectrum $S_{\mathcal{C}}$ as the associated maximal level-set in spectrum $S_{\mathcal{C}}$ [45], which does not contain other significant detected maxima, *i.e.* the greatest connected set of pixels of $S_{\mathcal{C}}$ above a given energy level which contains the considered local maximum and does not contain any other significant local maximum. Given this set of significant geometric patterns, we discriminate the geometric patterns which involve loop patterns from the other ones, as they may refer to different behaviours/processes [19]: a geometric pattern corresponds to a "looping" pattern with characteristic radius R if the associated segment along curve $\mathcal{C}_R$ contains self-intersections and as an "oscillating" pattern otherwise.

V. Application to wild animal movement pathes

We consider an example of a seabird (Peruvian booby, *Sula variegata*) foraging round trip off its colony (Guañape Sur island, Peru) during the breeding season (Fig.1, left). The track was recorded using a miniaturized GPS tag sampling positions every 1s (See Bertrand et al 2012 for further details). The application of the proposed framework first requires to resample the trajectory w.r.t. the curvilinear abscissa with a 10-meter resolution. We use $b_R = a_R/10$ in (Eq.3).

The scale-space geometry spectrum of the trajectory reveals the presence of looping and oscillating patterns at different scales, characterized by relatively high-level energy regions (Fig.5, upper right). Focusing on the looping patterns (Fig.5, left and upper right panels, magenta) which typically range from a few tens of meters to ten kilometers, the spectrum reveals nested patterns where small geometric structures are included in larger ones (Fig.5, lower right panel). For instance, at a curvilinear abscissa of 35km, the structure of 1 km radius includes a structure of a few hundreds of meters, itself comprising a structure of a few tens of meters. Our approach also delivers the distribution of the total energy across the geometric scales (Eq.5)) and reveals two main modes associated to structures of 300 m and 9 km radius (Fig.5, lower right panel).

Boobies in Peru mostly forage on Peruvian anchovy (Engraulis ringens), a highly gregarious pelagic fish, organized in nested collective structures: school, cluster of schools, clusters of cluster [22]. The nested patterns observed in the boobies tracks are consistent with possible sizes for schools (100s of m) and clusters of schools (few kms). These

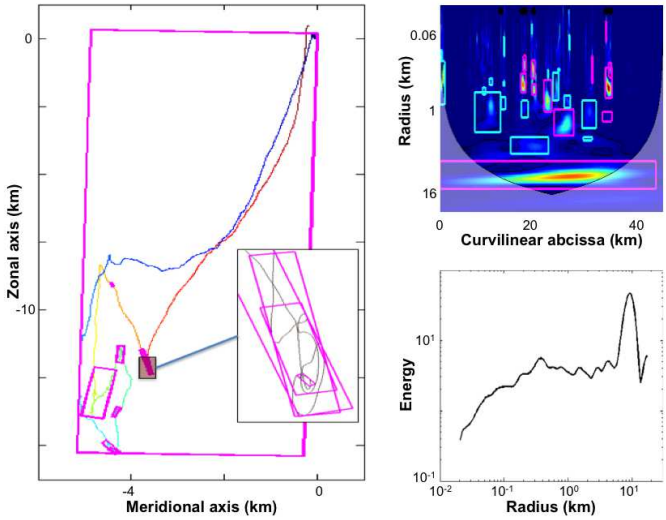

Fig. 5. **Multiscale analysis of the foraging trajectory of a seabird off its colony**: GPS track of the foraging trip of a Peruvian booby (*Sula variegata*) off Guañape island (Peru) depicting detected looping patterns (left), multiscale power spectrum of the geometry along the trajectory as well as detected looping (magenta) and oscillating (cyan) patterns (upper right panel), total energy distribution across scales (lower right panel).

results might reveal the behavioural adaption of boobies to the hierarchical nested structure of the prey schools in relation to forcing ocean features (eddies, fronts, upwelling regions). This example points out the relevance of our contribution compared to previous works [19], [23], [32], which only explore a predefined scale (see for example Fig.1). Such a quantitative characterization makes feasible the study of the potential relationships of seabird behaviors to the spatial distribution of the prey field [6].

VI. Application to ocean surface dynamics

The proposed framework also provides a novel approach for the multiscale analysis of geometric image deformations. More precisely, real-valued 2D fields or images can be fully represented by their level-lines[1]. Such a level-line-representation is contrast-invariant [45] and may be considered to characterize the geometry of the considered real-valued image or field. To our knowledge, only few works have investigated this potential. One may for instance cite an application to texture recognition [62] as well as our recent work for an application to satellite images of sea surface temperature (SST) [1]. Here, we aim at applying the proposed multiscale analysis of the geometry of planar curves to further investigate the extent to which we can reveal novel geometric features of remotely sensed geophysical fields.

From a thematic viewpoint, this level-line-based approach appears well suited for the characterization of ocean fronts from remote-sensing observations of geophysical fields at the ocean surface (e.g., temperature, salinity, ocean

[1]Given a real-valued image, a level-line for a given real value a is a planar curve such all points of the curve have the same value a in the image [45]. By construction, at any point along a level-line, the tangent to the level-line is orthogonal to the image gradient, such that level-lines locally match image contours, defined as large gradient segments.

color, current). Over the last decades, new satellite sensors have provided a wealth of relatively high-resolution information (typically, from a few kilometers to tens of kilometers) about ocean circulation and atmosphere-ocean interactions. Accordingly, our picture of upper ocean dynamics has considerably evolved towards a complex system characterized by strong multiscale interactions. It is now widely recognized that superimposed to the large-scale currents (horizontal scales of 100-1000 km), the ocean is populated of mesoscale eddies (10-100 km) and submesoscale structures ($<$10km) that dominate the kinetic energy of the ocean and play a major role for ocean-atmosphere exchanges or ocean biological dynamics [33]. Although numerous studies have been dedicated to the extraction and tracking of submeso- and meso-scale structures such as mesoscale eddies [12], [13], [14], frontal structures [3], [4], [47], or filaments [18], [60], very few works have explored beyond the Fourier spectrum laws [5] the statistical characterization of the geometrical signatures of these mesoscale dynamics. As mentioned by LaCasce and Mahadevan [37], one of the the most commonly used parameters to describe the mesoscale dynamics from spatial observations is the sea-surface height, whose horizontal gradients allows to compute the surface geostrophic velocities. However, sea-surface height provides surface geostrophic velocities only and the distances between altimeter satellite ground tracks and orbit revisit time are generally large (up to 200 km and 35 days, respectively) compared to other surface parameters observed from satellites such as SST or chlorophyll-a concentration. Thus, as an alternative to depict the dynamics of the upper oceanic layers from surface satellite observations, it has been recently proposed to use the Surface Quasi Geostrophic (SQG) theory which considers that the ocean dynamics is entirely driven by the surface density anomaly [29], [30], [33], [37], [38]. Except in localized regions where the ocean stratification is controlled by salinity changes (e.g. polar regions influenced by sea-ice melting/formation, near-coastal regions influenced by river estuaries, etc.), it can be considered that surface density fluctuations are at first order driven by SST changes [33], [38]. In this case, the application of the SQG theory using SST data may be used to reconstruct three-dimensional flows as illustrated in several regions of the World Ocean [30], [37] and in numerical simulations of baroclinic unstable flows similar to the Antarctic Circumpolar Current [38]. This method reveals the dynamics of the upper oceanic layers (0-500 m) for a spectral range extending from scales of O(10 km) to O(400 km) [38]. Thus, considering the SQG theory, the SST is no longer a passive tracer but an active one which directly influences the meso and submesoscale surface dynamics. These results strongly advocate for an in-depth exploration of the potential of a SST-driven characterization of mesoscale upper ocean dynamics.

In this respect, the analysis of the geometry of SST fields appears of key interest, as supported by recent theoretical advances in the field of turbulence [5]. More precisely, the geometry of the level-lines of advected tracer fields has been shown to depict specific fractal properties associated with intrinsic characteristics of the underlying turbulent dynamics for generic turbulence models [5]. Following these theoretical advances, we recently investigated fractal statistics of the level-lines of satellite SST images in active ocean regions [1]. Applied within the Agulhas region, an active boundary current region, we showed seasonal variations of these fractal statistics, which probably relate to the seasonal activity of the Aghulas current and Antarctic Circumpolar Current fronts (e.g. [17], [51], [52], [55]). Beyond fractal signatures, one may question whether or not SST fields involve geometric scale ranges, characteristic of the underlying ocean dynamics. Whereas the statistical characterization of mesocsale eddies is

well documented, e.g. [12], [14], mesoscale dynamics are also characterized by other structures, such as fronts or filamentary structures, whose geometric featrures remain less well known.

To this end, we further explore the extent to which the ocean mesoscale dynamics may be characterized by specific multiscale geometric patterns exhibited by the SST fields using the method developed in this paper. As in [1], we focus on the Agulhas region, whose dynamics and frontal characteristics have been extensively studied from in-situ data (e.g. [2], [35], [39]), satellite sea-surface height measurements (e.g. [51], [52], [53], [54]) and SST observations (e.g. [17], [36]). We here analyze weekly SST satellite maps (AMSRE data at a 25kmx25km resolution) over the 2003-2009 time-period, and proceed according to a three-step procedure:

- Step A: for each weekly SST map, we detect the level-line corresponding to the largest mean SST gradient [1] as illustrated for two particular maps in January 2003 and July 2003 (Fig.6, left). The geometry of this level-line can be regarded as representative of the mean geometrical signatures in the frontal area where the strong Antarctic Circumpolar Current is centered and mesoscale eddies are frequently observed [14], [51], [52];
- Step B: We compute, for each weekly map, the scale-space geometry spectrum of the level-line associated with the maximum SST gradient (Eq.4). We derive the weekly series, from 2003 to 2009, of the total energy distribution across scales of the geometric deformations (Eq.5);
- Step C: We derive the seasonal cycles of these multiscale geometric deformations by monthly averaging over this seven-year series.

The total energy distributions across scale of the geometric deformations for two dates (Fig.6, center) reveals that the frontal area involves much more geometric deformations in July 2003 than in January 2003 with three energetic scales between a few tens of kilometers to 100 km, between 100 km and 200 km and between 300 km and 400 km. In contrast, in January 2003, we observe a large mode from 10 km to 100 km and a second mode between 150 km and 350 km. Although the resolution of the AMSRE-SST observations may exclude the presence of characteristic patterns below a few tens of kms, scales from 10 km to 200 km probably relate to the presence and shedding of mesoscale eddies across the front, including filamentary structures (see Fig3, left panel) [12], [14]. Larger scales (300 to 400km) might reveal the large scale meandering of the front. From the analysis of drifters trajectories, Kort [34] also pointed out wavelike oscillations of the Antarctic Circumpolar Current jets, with wavelength up to 400 km. As we rely here on the analysis on weekly SST fields, we can further analyse seasonal variations. Interestingly the mean seasonal cycle (Fig.6, right) obtained from 2003 to 2009, clearly highlights two different regimes. Whereas previous studies evidenced seasonal frontal patterns in terms of North-South displacements and mean SST and gradient values (e.g., [17], [36]), our study points out that the studied frontal region also depicts seasonal variations in terms of observed scale ranges as well as in terms of deformation energy levels. During the austral winter (June-September) large deformation energies are observed for scales varying from 30 km to 300 km. In contrast during austral summer (December-March), lower energy values are observed and deformations are more likely associated with typical scales of 35-80 km. This seasonality is consistent with our previous study [1], which

revealed seasonal variations of the geometrical regularity of the SST fields in this region, and may also relate to the seasonality of the meandering of the front as reported in [55]. Although beyond the scope of this paper, future works should explore in more details the physical processes involved in the observed temporal variations and the types of structures associated with each characteristic scale range. In this respect, we may rely on the detection and tracking of the significant oscillation-like geometric patterns in the SST observation series as reported above for a seabird track.

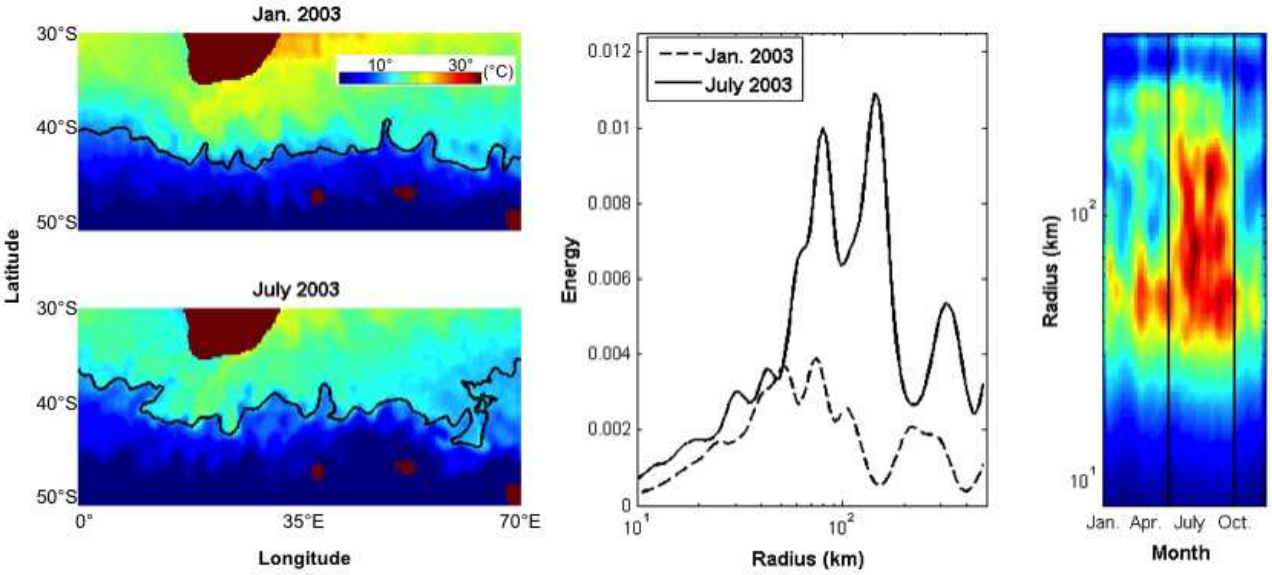

Fig. 6. **Multiscale analysis of the geometry of sea surface temperature (SST) observations in the Aghulas region off South Africa**: two SST observations from January and July 2003 and the analyzed front level-lines (left), energy distribution of the deformations across geometric scales from 10km to 500km (middle), seasonal cycle of the geometric deformations of the front level-lines computed as a mean over the weekly 2003-2009 AMSRE-SST series (right).

VII. Conclusion and future work

In this paper, we addressed the multiscale characterization of geometric structures along planar curves. We evidenced that existing approaches cannot address multiscale patterns. We proposed a scale-space decomposition of the geometric deformations along a planar curve based on a scale-space analysis of the local orientation of the curve. The resulting scale-space spectrum provided a quantitative characterization of the distribution of geometric deformations across scales. It was also exploited to extract significant local looping and oscillating structures along a curve. We reported an application to the analysis of GPS seabird trajectories and an application of the analysis of the geometry of 2D geophysical ocean surface fields. These applications emphasized the relevance of our contribution for the determination of characteristic geometric scales and the extraction of geometric patterns of interest, issues which cannot be addressed to our knowledge by previous methodologies.

Future works could explore and evaluate other types of time-frequency decompositions [20], in particular Wigner-Ville-like or EMD-like (Empirical Model Decomposition), for the analysis of planar curves' geometry. Our contribution also opens new research directions for the multiscale characterization of geometric deformations in images.

Using primitive-specific noise priors, it provides new means for addressing the multiscale extraction of geometric image primitives (e.g., wave-like patterns, straight lines,...) and could complement the numerous schemes dedicated to the detection of key points [43] and elementary geometric primitives (e.g., corners, t-junctions, edges,...) in images [16]. Texture analysis might also benefit from the proposed framework. Recently, simple statistics of texture level-sets were proven to deliver a powerful texture characterization [62]. The actual characterization of geometric patterns along level-lines of visual textures might supply relevant additional contrast-invariant features.

This paper proposed a novel scheme for the analysis of the geometry along individual trajectories. As illustrated, ongoing work further investigates their applications to the analysis of the foraging behaviour of top predators from GPS tracks. Other applications, in particular regarding surveillance issues (e.g., video surveillance, vessel monitoring, etc.) are also under consideration. Regarding upper ocean dynamics, the proposed methodology provides new means for the geometric characterization of the space-time variabilities of ocean fronts in remotely sensed geophysical fields (SSH, SST, ocean colour, salinity,....).

REFERENCES

[1] Ba, S., Autret, Chapron, B., Fablet, R. Statistical descriptors of ocean regimes from the geometric regularity of Sea Surface Temperature observations. *IEEE Geosc. Rem. Sens. Lett.*, 9(5):851-854, 2012.

[2] Belkin, I., Gordon, A.L. . Southern ocean fronts from the Greenwich meridian to Tasmanis. *J. Geophys. Res.*, 101, C2, 3675-3696, 1996.

[3] Belkin, I.M., O'Reilly, J.E. An algorithm for oceanic front detection in chlorophyll and SST satellite imagery. *Jal Mar. Res.*, 78:319-326, 2009.

[4] Belkin, I.M., Cornillon, P.C., Sherman, K. Fronts in Large Marine Ecosystems. *Progr. Oceanogr.*, 81:223-236, 2009.

[5] Bernard, D.,Boffetta, G., Celani, A., Falkovich, G. Conformal invariance in two-dimensional turbulence. *Nature Physics*, 2(2): 124-128, 2006.

[6] Bertrand, S., Diaz, E., Niquen, M. Interactions between fish and fisher's spatial distribution and behavior: the anchovy (Engraulis ringens) fishery of Peru. *ICES Jal Mar. Sc.*, 61: 1127-1136, 2004.

[7] Bertrand, S., et al. Scale-invariant movements of fishermen: The same foraging strategy as natural predators. *Ecol. App.*, 17: 331-337, 2007.

[8] Bertrand, S., R. Joo, et al. Competition for the same fish: Local depletion by the fishery can affect seabird foraging. *Jal App. Ecol.*, 49: 1168-1177

[9] Bronstein, A.M., et al. A Gromov-Hausdorff Framework with Diffusion Geometry for Topologically-Robust Non-rigid Shape Matching. *Int. Jal Comp. Vis.*, 89(2-3): 266-286, 2010.

[10] Budillon, A., Evangelista, A., Schirinzi, G. GLRT Detection of Moving Targets via Multibaseline Along-Track Interferometric SAR Systems, *IIEEE Geosc. Rem. Sens. Lett.*, 9(3):348-352, 2012.

[11] Calenge, C., Dray, S., Royer-Carenzi, M. The concept of animals' trajectories from a data analysis perspective. *Ecol. App.*, 4(1): 34-41, 2009.

[12] Chaigneau, A., Eldin, G., Dewitte, B. Eddy activity in the four major upwelling systems from satellite altimetry. *Progr. Oceanogr.*, 83, 117–123, 2009.

[13] Chaigneau, A., Gizolme, A., Grados, C. Mesoscale eddies off Peru in altimeter records: Identification algorithms and eddy spatiotemporal patterns. *Prog. Oc.*, 79:106–119, doi:10.1016/j.pocean, 2008.

[14] Chelton, D. B., Schlax, M. G., Samelson, R. M. Global observations of nonlinear mesoscale eddies. *Prog. Oceanogr.*, 91:167–216, doi:10.1016/j.pocean.2011.01.002, 2011.

[15] Chuang, G. C., Kuo, C., Wavelet descriptor of planar curves: theory and applications. *IEEE Trans. on Im. Proc.*, 5(1): 56-70, 1996.

[16] Desolneux, A., Moisan, L., Morel, J.M.. A Grouping principle and four applications. *IEEE Trans. Patt. An. Mach. Int.*, 25(4): 508-513, 2003.

[17] Dong, S., Sprintall, J., Gille, S. T. Location of the Antarctic Polar Front from AMSR-E Satellite Sea Surface Temperature Measurements. *Jal Phys. Oc.*, 36(11):2075–2089, 2006.

[18] d'Ovidio, F., López, C., Hernández-García, E., Fernández, V. Mixing structures in the Mediterranean sea from Finite-Size Lyapunov Exponents. *Geophys. Res. Lett.*, 31:L17203, 2004.

[19] Fauchald, P.,Torkild T. Using First-Passage Time in the analysis of area-restricted search and habitat selection. *Ecol.*, 84:282-288, 2003.

[20] Flandrin, P. Time-frequency/time-scale analysis. *Academic Press*, 1999.

[21] Flandrin, P., Goncalves, P., Rilling, G. Detrending and denoising with Empirical Mode Decompositions, *Proc. Eur. Conf. on Signal Proc., Eusipco'2004*, 1581-1584, Wien, sept. 2004

[22] Fréon, P., Misund, O.A. Dynamics of pelagic fish distribution and behaviour: effects on fisheries and stock assesment. *Blackwell Sc.*, 1999.

[23] Fritz, H., et al. Scale-dependent hierarchical adjustments of movement patterns in a long-range foraging seabird.*Proc. R. Soc. Lond. B* 270:1143-1148, 2003

[24] Grados, D., Fablet, R., Ballón, M., Bez, N., Castillo, R., Lezama, A., Bertrand, A. Multiscale analysis of the spatial interactions between ecosystem components from acoustic survey data: application of the Northern SCH off Peru. *Can. Jal Fish. Aq. Sc.*,69(4):740-754(1, 2012.

[25] Hampapur, A., et al. Smart video surveillance. *IEEE Sig. Proc. Mag.*, 22(2):38-51, 2005.

[26] Huang, X., et al. Shape Registration in Implicit Spaces using Information Theory and Free Form Deformations. *IEEE Trans. Patt. An. Mach. Int.*, 2006.

[27] Humphries, N., Queiroz, N., Dyer, J. R. M., Pade, N. G. Musyl, M. K. et al. Environmental context explains Lévy and Brownian movement patterns of marine predators. *Nature* 465:1066-1069, 2010.

[28] Isard, M., Blake, A. CONDENSATION: Conditional Density Propagation for Visual Tracking. *Int. Jal Comp. Vis.*, 29(1):5-28, 1998.

[29] Isern-Fontanet, J., Chapron, B., Lapeyre, G., Klein, P. Potential use of microwave sea surface temperatures for the estimation of ocean. *Geophys. Res. Lett.*, 33:L24608, doi:10.1029/2006GL027801, 2006.

[30] Isern-Fontanet, J., Lapeyre, G., Klein, P., Chapron, B., Hecht, M.W. Three-dimensional reconstruction of oceanic mesoscale currents from surface *J. Geophys. Res.*, 113:C09005, doi:10.1029/2007JC004692, 2008

[31] Jonsen, I. D., Myers, R.A. Meta-analysis of animal movements using state-space models. *Ecol.*, 84:3055-3063, 2003.

[32] Knell, A.S., Codling, E.A. Classifying area-restricted search (ARS) using a partial sum approach. *Theor. Ecol.*, 2011.

[33] Klein, P., Isern-Fontanet, J., Lapeyre, G., Roullet, G., Danioux, E. Chapron, B., Le Gentil S., Sasaki, H. Diagnosis of vertical velocities in the upper ocean from high resolution sea surface height. *Geophys. Res. Let.*, 36:12603, 2009.

[34] Kort, V.G.. Mesoscale variability of currents and temperature in the Southern Ocean from drifting buoys data. *Oceanology*, 21(3): 291–298, 1981.

[35] Kostianoy, A. G., Ginzburg, A. I., Lebedev, S. A., Frankignoulle, M., Delille, B. Fronts and mesoscale variability in the southern Indian Ocean as inferred from the TOPEX/POSEIDON and ERS-2 altimetry data. *Oceanology*, 43 (5):632–642, 2003.

[36] Kostianoy, A. G., Ginzburg, A. I., Lebedev, S. A., Frankignoulle, M., Delille, B. Fronts in the Southern Indian Ocean as inferred from satellite sea surface temperature data. *Jal Mar. Systems*, 45-55-73, 2004.

[37] LaCasce, J. H., Mahadevan, A. Estimating subsurface horizontal and vertical velocities from sea-surface temperature. *Jal Mar. Res.*, 64, 695–721, 2006.

[38] Lapeyre, G., Klein, P. Dynamics of the upper oceanic layers in terms of surface quasigeostrophy theory. *J. Phys. Ocean.*, 36:165–176, 2006.

[39] Legeais, J., Speich, S., Arhan, M., Ansorge, I., Fahrbach, E., Garzoli, S. and Klepikov, A. The baroclinic transport of the Antarctic Circumpolar Current south of Africa. *Geophys. Res. Lett.*, 32: doi: 10.1029/2005GL023271. issn: 0094-8276, 2005.

[40] Ma, J., Antoniadis, A., Le Dimet, F.-X. Curvelet-Based Snake for Multiscale Detection and Tracking of Geophysical Fluids, *IEEE Trans. on Geosc. Rem. Sens.*, 44(12):3626-3638, 2006.

[41] Mallat, S. A Wavelet Tour of Signal Processing. Academic Press, 2008.

[42] Meng, L., Carlson, C.F. Object Tracking Using High Resolution Satellite Imagery. *IEEE Jal of Sel. Top. in App. Earth Obs. and Rem. Sens.*, 5(1):146-152, 2012.

[43] K. Mikolajczyk, et al. A comparison of affine region detectors. *Int. Jal. of Comp. Vis.*, 65, 43-72, 2005.

[44] Mokhtarian, F.; Mackworth, A.K.. A theory of multiscale, curvature-based shape representation for planar curves. *IEEE Trans. on Patt. An. Mach. Int.*, 14(8):789-805, 1992.

[45] Monasse, P., Guichard, F. Fast Computation of a Contrast Invariant Image Representation. *IEEE Trans. on Im. Proc.*, 9: 860-872, 2000.

[46] Nathan, R. Movement Ecology Special Feature - Perspective. *Proc. Nat. Am. Soc., PNAS* 105(49): 19050-19051, 2008

[47] Nieto K., Demarcq, H., McClatchie S. Mesoscale frontal structures in the Canary upwelling system : new front and filament detection algorithms applied to spatial and temporal patterns. *Rem. Sens. Env.*, 123:339-346, 2012.

[48] Schell, S., Linder, S.P. Experimental Evaluation of Tracking Algorithms Used for the Determination of Fish Behavioral Statistics. *IEEE Trans on. Ocean. Eng.*, 31(3):672-684, 2006.

[49] Schouten, M.W., de Ruijter, W.P.M., van Leeuwen, P.J. Upstream control of Agulhas Ring shedding. *Jal Geophys. Res.*, 107:8, 3109, 2002.

[50] Sivic, J., Zisserman, A. Object Level Grouping for Video Shots. *Proc. Eur. Conf. on Computer Vision, ECCV'2004, LNCS 3022*:85-98, 2004.

[51] Sokolov, S., Rintoul, S.R. Circumpolar structure and distribution of the Antarctic Circumpolar Current fronts:1. Mean circumpolar paths.*J. Geophys. Res.*,114, C11018, doi:10.1029/2008JC005108, 2009.

[52] Sokolov, S., Rintoul, S.R. Circumpolar structure and distribution of the Antarctic Circumpolar Current fronts:2. Variability and relationship to sea surface height. *Jal Geophys. Res.*,, 114 , C11019, doi:10.1029/2008JC005248, 2009.

[53] Swart, S., Speich, S., Ansorge, S., Lutjeharms, J.R.E. An altimetry-based gravest empirical mode south of Africa: 1. Development and validation. *Jal Geophys. Res.*, doi:10.1029/2009JC005299, 2010.

[54] Swart, S., Speich, S. An altimetry-based gravest empirical mode south of Africa: 2. Dynamic nature of the Antarctic Circumpolar Current fronts, *Jal Geophys. Res.*, 115, C03003, doi:10.1029/2009JC005300, 2010.

[55] Tandeo, P., Chapron, B., Ba, S., Autret, E., Fablet, R. Segmentation of Mesoscale Ocean Surface Dynamics using SST and SSH Observations. Submitted to *IEEE Trans. on Geosc. Rem. Sens.*

[56] Tew Kai, E., V. Rossi, J. Sudre, H. Weimerskirch, C. Lopez, et al.. Top marine predators track Lagrangian coherent structures. *Proc. Nat. Am. Soc., PNAS*, 106(20): 8245-8250, 2009.

[57] Torrence, C., Compo, G.P. A Practical Guide to Wavelet Analysis. *Bull. Am. Met. Soc.*, 79: 61-78, 1998.

[58] Turchin, P. 1998. Quantitative analysis of movement. Measuring and modeling population redistribution in animals and plants. Sinauer Associates, Inc, 1998.

[59] Turchin, P. 1998. Spatial analysis of animals' movements using a correlated random walk model. Jal Th. Biol., 131:419-433.

[60] Waugh, D. W., Abraham, E.R. Stirring in the global surface ocean. *Geophys. Res. Lett.*,35:L20605, doi:10.1029/2008GL035526, 2008.

[61] Wilson, R.P., Liebsch, N., Davies, I., Quintana, F., Weimerskirch, H. et al. All at sea with animal tracks; methodological and analytical solutions for the resolution of movement. *Deep-Sea Research II*, 54:193-210, 2007.

[62] Xia, G.S., et al. Shape-based Invariant Texture Indexing, *Int. Jal Comp. Vis.*, 88(3): 382-403, 2010.

[63] Yang, X., et al. Improving shape retrieval by learning graph transduction. *Proc. Eur. Conf. on Comp. Vis., ECCV'2008, LNCS 5305*: 788-801, 2008.

[64] Zhang, D., Lu, G. A. Comparative study of curvature scale space and Fourier descriptors for shape-based image retrieval. *Jal Vis. Com. Im. Rep.*, 14(1): 41-60, 2003.